Hydrol. Earth Syst. Sci. Discuss., 8, 11519–11552, 2011
www.hydrol-earth-syst-sci-discuss.net/8/11519/2011/
doi:10.5194/hessd-8-11519-2011

Hydrology and Earth System Sciences Discussions

Flood frequency mapping of the middle Mahakam lowland area using satellite radar

H. Hidayat[1,2], D. H. Hoekman[3], M. A. M. Vissers[4], and A. J. F. Hoitink[1,5]

[1]Hydrology and Quantitative Water Management Group, Wageningen University, Wageningen, The Netherlands
[2]Research Centre for Limnology, Indonesian Institute of Sciences, Cibinong, Indonesia
[3]Earth System Science and Climate Change group, Wageningen University, The Netherlands
[4]SarVision BV, Wageningen, The Netherlands
[5]Institute for Marine and Atmospheric Research Utrecht, Department of Physical Geography, Utrecht University, Utrecht, The Netherlands

Received: 2 December 2011 – Accepted: 13 December 2011 – Published: 22 December 2011

Correspondence to: H. Hidayat (hidayat.hidayat@wur.nl)

Published by Copernicus Publications on behalf of the European Geosciences Union.

Abstract

Floodplain lakes and peatlands in the middle Mahakam lowland area are considered as an ecologically important wetland in East Kalimantan, Indonesia. However, due to a lack of data, the hydrological functioning of the region is still poorly understood. Among remote sensing techniques that can increase data availability, radar is well-suitable for the identification, mapping, and measurement of tropical wetlands, for its cloud unimpeded sensing and night and day operation. Here we aim to extract flood extent and flood frequency information from a series of radar images of the middle Mahakam lowland area. We explore the use of Phased Array L-band Synthetic Aperture Radar (PALSAR) imagery for observing flood inundation dynamics by incorporating field water level measurements. Water level measurements were carried out along the river, in lakes and in peatlands, using pressure transducers. For validation of the open water flood frequency map, bathymetry measurements were carried out in the main lakes. A series of PALSAR images covering the middle and lower Mahakam area in the years 2007 through 2010 was collected. A fully inundated region can be easily recognized on radar images from a dark signature. Open water flood frequency was mapped using a threshold value taken from radar backscatter of the permanently inundated river and lakes area. Radar backscatter intensity analysis of the vegetated floodplain area revealed consistently high backscatter values, indicating flood inundation under forest canopy. We used those values as the threshold for flood frequency mapping in the vegetated area.

1 Introduction

Flood frequency maps are an important source of input for integrated assessment of flood dynamics, ecological processes, and vulnerability, required in planning, designing, and operating flood works, nature reserves, and land management policies (Qi et al., 2009). Regular acquisition of remotely sensed inundation extents allows us to

Discussion Paper | Discussion Paper | Discussion Paper | Discussion Paper |

HESSD

8, 11519–11552, 2011

Flood frequency mapping of a tropical lowland

H. Hidayat et al.

map flood frequencies over a large area. In areas with less cloud cover, data from optical sensors such as Landsat imagery can be used for this purpose (e.g. Qi et al., 2009; Ran and Lu, 2011). Ran and Lu (2011) noted that images with cloud cover of less than 5 % are preferred. However, for the humid tropics area, the preferred limit of cloud cover is hard or even impossible to be satisfied.

Radar imagery is useful for the identification, mapping, and measurement of streams, lakes, and wetlands in humid tropic areas as it is unconstrained by cloud cover (Romshoo, 2006; Henderson and Lewis, 2008; Hoekman, 2009). Most surface water features are detectable on radar imagery because of the contrast in return between the smooth water surface and the rough land surface (Lewis, 1998). The advantages of using space-borne radar in environmental monitoring in these areas are that radar measurements can remotely acquire data in poorly accessible areas with 24 h per day functioning, and to a certain extent, that radar can penetrate vegetation cover. The latter functionality allows to observe flooding under a closed forest canopy. Detection of flooded forest is enabled by the bright appearance of the inundated forest on radar images as a result from double bounce reflections between water surfaces and tree trunks or branches (Hess et al., 1990).

The Phased Array L-band Synthetic Aperture Radar (PALSAR) is one of the remote sensing instruments onboard of the Advanced Land Observing Satellite (ALOS). PALSAR is a polarimetric instrument operating at a wavelength of 23.6 cm with a 46-day satellite cycle period for global environmental monitoring (Rosenqvist et al., 2007). The modes of observation include Fine Beam Single Polarization (FBS), Fine Beam Dual Polarization (FBD), Polarimetric (POL), and ScanSAR. FBS and FBD are designed for land cover changes and forest monitoring. POL is dedicated to research related to polarimetry and polarimetric interferometry. ScanSAR is intended for seasonal phenomena studies such as inundation extent monitoring and rice-field mapping. All land areas on the globe are covered at least once every year by the FBS, FBD, and ScanSAR modes. The typical repetition frequency for most areas is three to five times per year (Rosenqvist et al., 2007).

HESSD
8, 11519–11552, 2011

The application of remote sensing and GIS plays an important role in filling the gaps in wetland inventory and could reduce uncertainties due to data availability constraints (Rebelo et al., 2009). Radar data sets are gradually obtaining a more prominent role in wetland mapping, not only in scientific projects but also in operational practices that require information on wetlands' presence, extent, and conditions (Henderson and Lewis, 2008). SAR technology has been used for remote monitoring of inundation patterns, duration of hydroperiods and computation of surface water level changes in the Everglades wetlands in Florida (Bourgeau-Chavez et al., 2005; Wdowinski et al., 2008). Rosenqvist and Birkett (2002) investigate the hydrological applications of JERS-1 SAR mosaics in the Congo river basin. They proposed that SAR mapping missions need at least three repetitive observations within one year to describe the hydrology in such a complex region. Recently, Salvia et al. (2011) used Envisat ASAR and AMSR-E data to estimate the fraction of flooded area and mean water level in the wetland of the Parana River Delta floodplain. They found that both active and passive microwaves data can be used to estimate water level in flooded vegetation. The specular reflection of microwaves from open smooth water bodies resulting in dark tones on the SAR image can be used to evaluate 1-D or 2-D flood inundation models (Schumann et al., 2008).

This study explores the use of PALSAR imagery for floodplain dynamics mapping of the Mahakam River Basin (MRB). The MRB is located in Kalimantan, the Indonesian part of Borneo, between 2° N to 1° S and 113° E to 118° E. It represents a poorly gauged meso-scale river basin with a complex land cover mosaic. Part of the runoff that feeds the Mahakam is derived from peat domes, which are difficult to monitor. In studies at the plot scale, piezometers are commonly used to analyze water levels in peat, which are labour intensive to maintain (Devito et al., 1996; Baird et al., 2004; Fraser et al., 2001). Combination of SRTM data, time-series of radar images and field measurement can be applied to study the temporal dynamics of the lake water mixture, and the fluxes between the river and the floodplain adjacent to the river (Bonnet et al., 2008). Using the difference in mean brightness levels from SIR-B L-band radar image of coastal lowland in East Kalimantan, Ford and Casey (1988) characterized three classes of forest canopy (swamp, coastal lowland forest and tidal forest) and two classes of open land cover (wetland and clear cuts). Ford and Casey (1988) also noted the enhanced backscatter returns from the inundated area covered by mangrove and nipah swamps. Time-series of L-band radar data such as the JERS-1 SAR, the predecessor of PALSAR, have been applied to acquire information on the hydrology in Central Kalimantan peat swamps (Hoekman, 2007).

Hoekman et al. (2010) used PALSAR images of 2007, which covered the whole of Borneo, for land use/land cover mapping based on the classification of FBS and FBD polarization (path) image pairs. They obtained good results for a sub-continental high resolution map, except for grassland, cropland and shrubland. The obtained land use/land cover (LULC) map had an accuracy of 85.5 % full agreement and 7.8 % partial agreement with the independent reference dataset. Application of longer or denser time-series were expected to improve results significantly. Figure 1 shows the LULC map of Borneo zoomed in on the MRB area. The middle Mahakam region has a complex land cover mosaic that mainly consists of degraded forest, riverine forest, shrub, agriculture area, swamp and peat forest, which is strongly related to the inundation pattern and anthropogenic disturbances.

In this study we aim to extract flood extent and flood frequency information from a series of radar images of the middle Mahakam lowland area, including both open water and areas under vegetation. The remainder of this paper is structured as follows. Section 2 describes the study area and a brief hydrological background of the middle Mahakam area. Descriptions of data collection and data processing are presented in Sect. 3. Section 4 presents the results discussion and finally Sect. 5 presents the conclusions.

HESSD
8, 11519–11552, 2011

2 Study area

The Middle Mahakam Area (MMA) is characterized by low relief (Fig. 2) with around 40 shallow lakes on both sides of the river. Lakes Semayang, Melintang, and Jempang are the three largest lakes in this region. Lakes in the MMA regulate the discharge in the lower Mahakam area. They have a function as a buffer by storing water during the high flow conditions, and releasing it during low flows. Lake filling and emptying mechanisms play a role to shave water level peaks downstream of the Mahakam lakes area (Hidayat et al., 2011b). The MMA is also surrounded by peatland, as part of the Kutai lowland spreading over an area of 35 km NW-SE by 130 km SW-NE, with elevations of around sea level in the Mahakam River to ca. 24 m a.s.l. (Hope et al., 2005). The peat in Kalimantan is of the ombrogenous type (Jaenicke et al., 2010; Page et al., 2004). This type of land potentially stores more water than any other type of land because of the sponge nature of the pores.

The climate in Kalimantan is highly influenced by the Indo-Australian Monsoon driven by the Inter-tropical Convergence Zone, and El Nino-Southern Oscillation (Meehl and Arblaster, 1998). A record from a meteorological station in Kotabangun in the Central part of the MMA showed that in general, the mean daily temperature varies between 24 and 29 °C, relative humidity between 73–99 % and the mean annual precipitation is approximately 2300 mm. During El Nino-Southern Oscillation (ENSO) years such as in 1997, precipitation can be as low as nearly a half of the mean annual record. Due to the global air circulation and the regional climate, the Mahakam catchment has a bimodal rainfall pattern with two peaks of rainfall, which generally occur in December and in May. The normal dry season lasts from June to September. However, it may begin as early as March and last until November, as was the case during the ENSO event in 1997.

The flooding regime in the MMA is generally characterised by long duration floods during the peak of the rainy season in December through January and in May, with some short duration high water events in between. Water levels at the upstream

HESSD
8, 11519–11552, 2011

stations are fluctuating primarily in response to rainfall in the catchment, while more downstream they are also influenced by the tidal motion. Bank overtopping occurs during a flood situation in Penyinggahan (Fig. 3). During this period, the Penyinggahan floodplain is flooded and water flows through the floodplain to Lake Melintang, then to Lake Semayang, and finally meets the Mahakam again through a tie-channel. Downstream of the middle Mahakam area, water level fluctuation is relatively low. Beside the lakes, the vast area of the Kutai wetland is believed to also control the River Mahakam water level and discharges downstream. The information on flood duration and inundation extent obtained in the context of the present study will be used in a future stage to model the hydrological functioning of the area, which has not been quantified to date.

3 Methodology

A series of PALSAR images with HH polarity and a pixel spacing of 75 m was provided by the Japan Aerospace Exploration Agency (JAXA), covering the middle and lower Mahakam areas for the years 2007 through 2010 (Table 1). The PALSAR images were radiometrically calibrated, orthorectified using 3$''$ SRTM data and corrected for slope illumination effects. Next, these geocoded data were chronologically stacked into a layered multi-temporal radar image suitable for time-series analysis. Figure 4 shows the spatial and temporal dynamics of radar backscatter from PALSAR images of the study area during wet and dry seasons. These dynamics are related to flood conditions and soil moisture.

The flood frequency was determined by evaluating pixels in the images used as input against the lower and the upper threshold values. The pixel was flagged as flooded if its backscatter value falls within the range of the lower and upper thresholds. An image with pixel values of counts of the flooded flag was obtained, which was then color mapped. As radar returns for flooding in open areas and for flooding under vegetation result in contrasting behavior (dark for the former and bright for the latter), the two

HESSD
8, 11519–11552, 2011

types of flooding were mapped separately. From the input images we acquired radar backscatter statistics in regions covering the main river and lakes that are known to be permanently inundated, to determine threshold values for open water flood frequency mapping. The minimum was taken as the lower threshold, and mean plus one standard deviation was taken as the upper threshold. For flooding under vegetation cover, we determined the threshold from backscatter statistics obtained from the floodplain region. The mean was taken as the lower threshold, and the maximum was taken as the upper threshold. Based on Hope et al. (2005), we mapped flood frequency of the MMA with elevation of less than 24 m a.s.l., as shown in Fig. 2. The downstream end of the mapped area is the region of Senoni village, where the relief shifted to a steeper terrain that marks the difference in geological settings of the downstream region.

Speckle filtering was applied prior to flood frequency mapping. In a preliminary flood frequency map derived from unfiltered images, contours of the river and lake extent, which coincide with the circumferences of the areas with maximum flood frequency, was rather noisy. The enhanced Lee filter was used to reduce speckle in the radar images while preserving texture information. The enhanced Lee filter uses coefficients of variation within individual filter windows. All pixels are divided into three classes: homogeneous, heterogeneous, or point target. Each class type is treated differently. The pixel value is replaced by the average of the filter window, replaced by the weighted average, or is not changed for homogeneous, heterogeneous, and point target classes, respectively (Lopes et al., 1990).

Pressure transducers to measure water levels were installed in the peat forest near Lake Melintang, at the shrub-covered peat swamp floodplain in Penyinggahan, along the river in Melak (upstream of MMA) and in Muara Kaman (downstream of MMA), and in the main lakes (Jempang, Semayang, Melintang). Local flood levels at the water level gauge locations were determined by evaluating the relative position of the pressure transducers and water levels to the ground surface. Bathymetry data of lakes were collected using a single beam echosounder.

HESSD
8, 11519–11552, 2011

4 Results and discussion

4.1 Water level and radar backscatter relationship

An analysis of the relationship between radar backscatter and water levels is reported in Hidayat et al. (2011a). For lakes and shrub covered peatland, where the range of water level variation was large, a high water level-backscatter correlation was obtained. In forest covered peatland subject to a small range of water level variation, water level-backscatter correlations were poor. Poor correlation between water level and radar backscatter for this area could be related to the limitation of PALSAR over certain thresholds of biomass on the forest canopy.

Radar backscatter intensity depends on land cover type. The land use – land cover map by Hoekman et al. (2010) identified 19 classes of land cover types. Figure 5 shows time-series radar backscatter intensity for several key land cover types in the middle Mahakam area, revealing a markedly diverging response to flooding. Regularly inundated medium shrub and high shrub were very sensitive to flooding, yielding low backscatter returns when fully inundated. Other land cover classes representing vegetated areas generally feature a moderate increase of radar backscatter intensity with flood inundation.

4.2 Temporal analysis of PALSAR data

A temporal analysis of radar backscatter was carried out based on the statistics from 20 images. A standard deviation image captures the backscatter intensity standard deviation for all pixels in the image. From the maximum and minimum value of radar backscatter we obtained the range image. The average absolute difference of consecutive images resulted in the mean change image. The color composite of the latter three images (Fig. 6) reveals a zoning that provides details in an area that was poorly classified in the work of Hoekman et al. (2010), for its complexity. The map shows land cover types that are related to the dynamics of inundation, i.e. the regularly inundated

HESSD
8, 11519–11552, 2011

shrubland, reeds/sedges growing during dry season and floating vegetation such as water hyacinth in lake areas, and rice growing in lake areas in years when flood levels are not too high.

From the mean of three images representing the wettest conditions, we obtained a map with the maximum inundation extent of the MMA, covering inundated areas in both open water and in vegetated areas. Figure 7 shows that a vast area of the MMA is inundated during the flood conditions, including villages along the Mahakam river and floodplain area, which appear as open water. The open water inundation extent was indicated by dark radar returns. Flooding under vegetation showed bright radar returns that was colour mapped in Fig. 7 to distinguish it from other extent.

4.3 Flood frequency mapping of open water extent

Nine images from 2008 through 2009 were used to make a flood frequency map, and served as the basis for accuracy assessment using field measurements taken in the corresponding period. Figure 8 shows the flood frequency map of the MMA from nine filtered PALSAR images using the threshold value of −25.1 to −11.2 dB (taken from the mean backscatter value of the permanently inundated lake). Permanently inundated lake areas and main river sections were well-mapped with the maximum probability of flood frequency. During the peak flooding events in the rainy seasons in May 2008 and December 2008, a vast area of the MMA is inundated, including villages and cities along the river. These radar-inferred flood events were qualitatively confirmed by flood marks on houses and trees in the study area, besides water level records from pressure sensors. Quantitatively, the open water flood frequency was validated using data from bathymetry measurements of lakes (Fig. 9) taken during the high water period in March 2009. Flood frequency was sampled from the flood frequency map along the bathymetric track by extracting values on the map at the respective depth sampling point. Overall, flood frequency was well-correlated with lake depth (Fig. 10), deeper areas were more frequently flooded than shallower areas at the shore and near islands.

At some places, emergent and floating plants could occupy large and patchy parts of the lakes, especially in the shallower area, creating abrupt changes in flood frequency between neighboring cells.

To investigate the MMA hydrological dynamics in different temporal coverages, open water flood frequency maps were produced further using 20 images from 2007–2010, with the same threshold values. Flooding extents are generally similar between the two flood frequency maps. However, significant differences were observed when zooming into the lakes area (Fig. 11), compared with the 2008–2009 flood frequency for the same location in Fig. 9. Table 2 shows the correlation between lake depth and flood frequency for the two flood frequency maps. Depth-frequency correlations remained relatively high for Lake Melintang but dropped for all bathymetry sections in Lake Jempang. This may be attributed to the stronger influence of human activity in Lake Jempang relative to Lake Melintang. During the dry season, large parts of Lake Jempang are used by local farmers to grow rice. This agricultural activity is not suitable in Lake Melintang due to the low pH values of water generated from peat forest. Compared to 2007, 2008 was a wet year and continued to remain wet in the first half of 2009, which resulted in relatively high lake water levels so that rice growing was not possible. In the second half of 2009, however, a relatively long dry period occurred. In addition, floating and emergent aquatic vegetations grow fast during the dry season and, to some extent, are maintained by local fishermen in Lake Jempang as nesting media for fish. During the lake emptying period following the end of the flood event, large parts of the floating plants were flushed downstream as a drifting bulk of biomass (Fig. 12). These vegetation dynamics and anthropogenic factors hindered validation of flood frequency maps using lake bathymetry data.

4.4 Flood frequency mapping of area under vegetation

It requires a large effort to map flooding under forest canopy, considering the poor correlation between radar backscatter and water level under such circumstances. An image obtained from combining the minimum, mean, and maximum backscatter values of 20 PALSAR images from 2007 to 2010 shows a clear signature of flooding under vegetation in the Mahakam floodplain, upstream of the MMA. The frequency of flooding under vegetation was obtained by frequency mapping the filtered images using the threshold value of -7.52 to -2.26 dB, taken from the mean and maximum of backscatter values of the regularly inundated floodplain upstream of the MMA. Figure 13 shows (ground) water level records at the peat forest near Lake Semayang, plotted along with radar backscatter values, which shows enhanced radar backcatter in this flooded forest. Backscatter values are relatively high during the wet period and relatively low during the dry period, except for the image acquired on 21 September 2008, which coincided with the dry period. For the latter image, backscatter values at the water gauging points were high for low water level conditions. This may relate to the relatively high soil moisture of the peat forest compared to the rest of the area, which could lead to a false detection of flood under vegetation. Flood detection in the shrub covered peat swamp is more problematic due to the dynamics in water levels and vegetation cover. On the one hand, shrub vegetations that are mainly reed and sedges grow and cover this area during the dry season. On the other hand, this area is fully inundated during the high water period, such that it becomes an extension of the lakes. When the flood recedes, shrub vegetation were fallen and the vegetation succession starts again. Consequently, some of underestimation and or overestimation of the inundated areas cannot be avoided, as noted previously by Romshoo (2006). Figure 14 shows the composite flood frequency map of the MMA, overlaying results for open water and for inundation under vegetation. The flood frequency of the peat swamps in Fig. 14 was mapped using the open water results, which neglects flooding of the peat areas under vegetation. This problem was solved by using a simple procedure to count the total number of flood cases per pixel, which represents open water and flooding under vegetation canopy (Fig. 15).

The flooding under vegetation frequency estimates were validated using water level measurement taken in the peat forest near Lake Melintang, by checking if the

HESSD
8, 11519–11552, 2011

radar-based assessments could be confirmed from the level gauges. The local gauge location is assumed to represent the complete pixel area, which features local topographic irregularities. Consequently, the gauge location may better represent one of the eight pixels surrounding the pixel in which the gauge is located. Figure 13 therefore shows the mean, minimum and maximum backscatter return values within a block of nine pixels at the gauge location, relative to the flooding under vegetation threshold line, and compares those values with the water level relative to the local ground level. In 78 % of the cases, radar-based assessments from one or more of the nine pixels correctly indicated the water level to be above or below the ground level. This gives merely a rough indication of the quality of the flood under vegetation frequency, at least showing radar backscatter to offer a promising means of monitoring flooding under vegetation. A much larger suite of level gauges and detailed information about the micro topography would be required to achieve a more quantitative accuracy assessment.

5 Conclusions

Flood extent and flood frequency information were inferred from a series of radar images of the middle Mahakam lowland area. Relative radar backscatter levels sampled in regions of interest and a land use/land cover map showed that different land cover types yield markedly different backscatter returns in response to flooding. Regularly inundated medium shrub and high shrub were sensitive to flooding, with decreasing radar backscatter during flood periods, while peat forest, riverine forest and tree plantation signatures featured a slight increase of radar backscatter with flood inundation.

Image statistics of the river and main lakes area were used to determine thresholds to map open water flood frequency. The minimum was taken as the lower threshold, and the mean plus or minus a standard deviation was taken as the upper or lower threshold (respectively). The bathymetry of lakes obtained during a high water period served as validation data for the open water flood frequency map. High correlations between lake depth and flood frequency were obtained for the map derived for wet year of 2008–2009, which is the period when field surveys were carried out. For the map derived from input images of 2007–2010, covering a longer dry period, the correlation between lake depth and flood frequency dropped for one particular lake, which was subject to high vegetation dynamics and rice growing activity. In a separate procedure, the average radar backscatter value of the floodplain area was used as a threshold to map flooding under forest canopy. Validation with water level data gave an indication that the flood frequency map under vegetation cover is fairly accurate.

The flood frequency map obtained from a newly developed algorithm offers a detailed insight into the hydroperiod and flood extent of the Mahakam lowland area, illustrating the added value of radar remote sensing to wetland hydrology. As a side effect, we found that simple statistics of the radar backscatter maps such as mean, total range and mean change can be used to improve land classification maps. This may help future efforts to classify flat and complex wetland areas such as the one under study, where existing classification methods fall short.

Acknowledgements. This research has been supported by the Netherlands organization for scientific research (NWO grant number WT76-268). This work has been undertaken in part within the framework of the ALOS Kyoto & Carbon Initiative. ALOS PALSAR data have been provided by JAXA EORC. The help from Maximiliano Sassi and Bart Vermeulen (Wageningen university), Fajar Setiawan and Unggul Handoko (LIPI-Limnology), Ulfah Karmilasari and Supriadi (Mulawarman University) in data collection is gratefully acknowledged.

References

Baird, A. J., Surridge, B. W. J., and Money, R. P.: An assessment of the piezometer method for measuring the hydraulic conductivity of a *Cladium mariscus–Phragmites australis* root mat in a Norfolk (UK) fen, Hydrol. Process, 18, 275–291, 2004. 11522

Bonnet, M. P., Barroux, G., Martinez, J. M., Seyler, F., Moreira-Turcq, P., Cochonneau, G., Melack, J. M., Boaventura, G., Maurice-Bourgoin, L., Leon, J. G., Roux, E., Calmant, S.,

HESSD

8, 11519–11552, 2011

Flood frequency mapping of a tropical lowland

H. Hidayat et al.

Kosuth, P., Guyot, J. L., and Seyler, P.: Floodplain hydrology in an Amazon floodplain lake (Lago Grande de Curuai), J. Hydrol., 349, 18–30, 2008. 11522

Bourgeau-Chavez, L. L., Smith, K. B., Brunzell, S. M., Kasischke, E. S., Romanowicz, E. A., and Richardson, C. J.: Remote monitoring of regional inundation patterns and hydroperiod in the Greater Everglades using synthetic aperture radar, Wetlands, 25, 176–191, 2005. 11522

Devito, K. J., Hillb, A. R., and Roulet, N.: Groundwater-surface water interactions in headwater forested wetlands of the Canadian Shield, J. Hydrol., 181, 127–147, 1996. 11522

Ford, J. P. and Casey, D. J.: Shuttle radar mapping with diverse incidence angles in the rainforest of Borneo, Int. J. Remote Sens., 5, 927–943, 1988. 11523

Fraser, C. J. D., Roulet, N. T., and Lafleur, M.: Groundwater flow patterns in a large peatland, J. Hydrol., 246, 142–154, 2001. 11522

Henderson, F. M. and Lewis, A. J.: Radar detection of wetland ecosystems: a review, Int. J. Remote Sens., 29, 5809–5835, doi:10.1080/01431160801958405, 2008. 11521, 11522

Hess, L. L., Melack, J. M., and Simonett, D. D. S.: Radar detection of flooding beneath the forest canopy: a review, Int. J. Remote Sens., II, 1313–1325, 1990. 11521

Hidayat, Hoekman, D. H., Vissers, M. A. M., and Hoitink, A. J. F.: Combining ALOS-PALSAR imagery with field water level measurements for flood mapping of a tropical floodplain, SPIE 8286, Proc. Int. Symp. on LIDAR and Radar Mapping: Technologies and Applications, Nanjing, China, doi:10.1117/12.912735, 2011a. 11527

Hidayat, H., Vermeulen, B., Sassi, M. G., Torfs, P. J. J. F., and Hoitink, A. J. F.: Discharge estimation in a backwater affected meandering river, Hydrol. Earth Syst. Sci., 15, 2717–2728, doi:10.5194/hess-15-2717-2011, 2011b. 11524

Hoekman, D. H.: Satellite radar observation of tropical peat swamp forest as a tool for hydrological modelling and environmental protection, Mar. Freshw. Ecosyst., 17, 265–275, 2007. 11523

Hoekman, D. H.: Monitoring tropical peat swamp deforestation and hydrological dynamics by ASAR and PALSAR, in: Geoscience and Remote Sensing, In-Tech, Vienna, 257–275, 2009. 11521

Hoekman, D. H., Vissers, M. A. M., and Wielaard, N.: PALSAR Wide-area mapping of Borneo: methodology and validation, IEEE J. Sel. Topics Appl., 3, 605–617, 2010. 11523, 11527, 11538

Hope, G., Chokkalingam, U., and Anwar, S.: The stratigraphy and fire history of the Kutai Peatlands, Kalimantan, Indonesia, Quaternary Res., 64, 407–417, 2005. 11524, 11526

Jaenicke, J., Wösten, H., Budiman, A., and Siegert, F.: Planning hydrological restoration of peatlands in Indonesia to mitigate carbon dioxide emissions, Mitig. Adapt. Strateg. Global Change, 15, 223–239, doi:10.1007/s11027-010-9214-5, 2010. 11524

Lewis, A. J.: Geomorphic and hydrologic applications of active microwave remote sensing in principles and application of imaging radar, in: Manual of Remote Sensing, vol, 2, John Wiley & Sons Inc., New York, 567–618, 1998. 11521

Lopes, A., Touzi, R., and Nezry, E.: Adaptive speckle filters and scene heterogeneity, IEEE T. Geosci. Remote Sens., 28, 992–1000, 1990. 11526

Meehl, G. and Arblaster, J.: The Asian-Australian Monsoon and El Nino-Southern oscillation in the NCAR climate system model, J. Climate, 11, 1356–1385, 1998. 11524

Page, S. E., Wust, R. A. J., Weiss, D., Rieley, J. O., Shotyk, W., and Limin, S. H.: A record of Late Pleistocene and Holocene carbon accumulation and climate change from an equatorial peat bog (Kalimantan, Indonesia): implications for past, present and future carbon dynamics, J. Quarternary Sci., 19, 625–635, doi:10.1002/jqs.884, 2004. 11524

Qi, S., Brown, D. G., Tian, Q., Jiang, L., Zhao, T., and Bergen, K. M.: Inundation extent and flood frequency mapping using LANDSAT imagery and digital elevation models, GISci. Remote Sens., 46, 101–127, doi:10.2747/1548-1603.46.1.101, 2009. 11520, 11521

Ran, L. and Lu, X. X.: Delineation of reservoirs using remote sensing and their storage estimate: an example of the Yellow River basin, China, Hydrol. Proc., in press, doi:10.1002/hyp.8224, 2011. 11521

Rebelo, L. M., Finlayson, C. M., and Nagabhatla, N.: Remote sensing and GIS for wetland inventory, mapping and change analysis, J. Environ. Manage., 90, 2144–2153, 2009. 11522

Romshoo, S. A.: Radar remote sensing for monitoring of dynamic ecosystem processes related to biogeochemical exchanges in tropical peatlands, Vis. Geosci., 9, 9–28, doi:10.1007/s10069-003-0015-9, 2006. 11521, 11530

Rosenqvist, A. and Birkett, C. M.: Evaluation of JERS-1 SAR mosaics for hydrological applications in the Congo River basin, Int. J. Remote Sens., 23, 1283–1302, 2002. 11522

Rosenqvist, A., Shimada, M., Ito, N., and Watanabe, M.: ALOS PALSAR: a pathfinder mission for global-scale monitoring of the environment, IEEE T. Geosci. Remote Sens., 45, 3307–3316, 2007. 11521

Salvia, M., Grings, F., Ferrazzoli, P., Barraza, V., Douna, V., Perna, P., Bruscantini, C., and Karszenbaum, H.: Estimating flooded area and mean water level using active and passive microwaves: the example of Paraná River Delta floodplain, Hydrol. Earth Syst. Sci., 15,

Discussion Paper | Discussion Paper | Discussion Paper | Discussion Paper |

2679–2692, doi:10.5194/hess-15-2679-2011, 2011. 11522

Schumann, G., Pappenberger, F., and Matgen, P.: Estimating uncertainty associated with water stages from a single SAR image, Adv. Water Sci., 31, 1038–1047, 2008. 11522

Wdowinski, S., Kim, S.-W., Amelung, F., Dixon, T. H., Miralles-Wilhelm, F., and Sonenshein, R.: Space-based detection of wetlands' surface water level changes from L-band SAR interferometry, Remote Sens. Environ., 112, 681–696, 2008. 11522

HESSD

8, 11519–11552, 2011

Flood frequency mapping of a tropical lowland

H. Hidayat et al.

Table 1. PALSAR images used in this study.

Image No.	PALSAR data dates
1	19 March 2007
2	4 May 2007
3	4 August 2007
4	19 September 2007
5	4 November 2007
6	20 December 2007
7	4 February 2008
8	21 March 2008
9	6 May 2008
10	21 June 2008
11	6 August 2008
12	21 September 2008
13	22 December 2008
14	9 May 2009
15	24 September 2009
16	9 February 2010
17	27 March 2010
18	12 May 2010
19	27 June 2010
20	27 September 2010

HESSD
8, 11519–11552, 2011

Flood frequency mapping of a tropical lowland

H. Hidayat et al.

Table 2. Correlation between lake depth and flood frequency mapped using different periods of PALSAR images for lake sections depicted in Fig. 9.

Period of images	# images	r_{A-B}	r_{C-D}	r_{E-F}	r_{G-H}
2008–2009	9	0.85	0.84	0.83	0.83
2007–2010	20	0.39	0.41	0.54	0.82

HESSD
8, 11519–11552, 2011

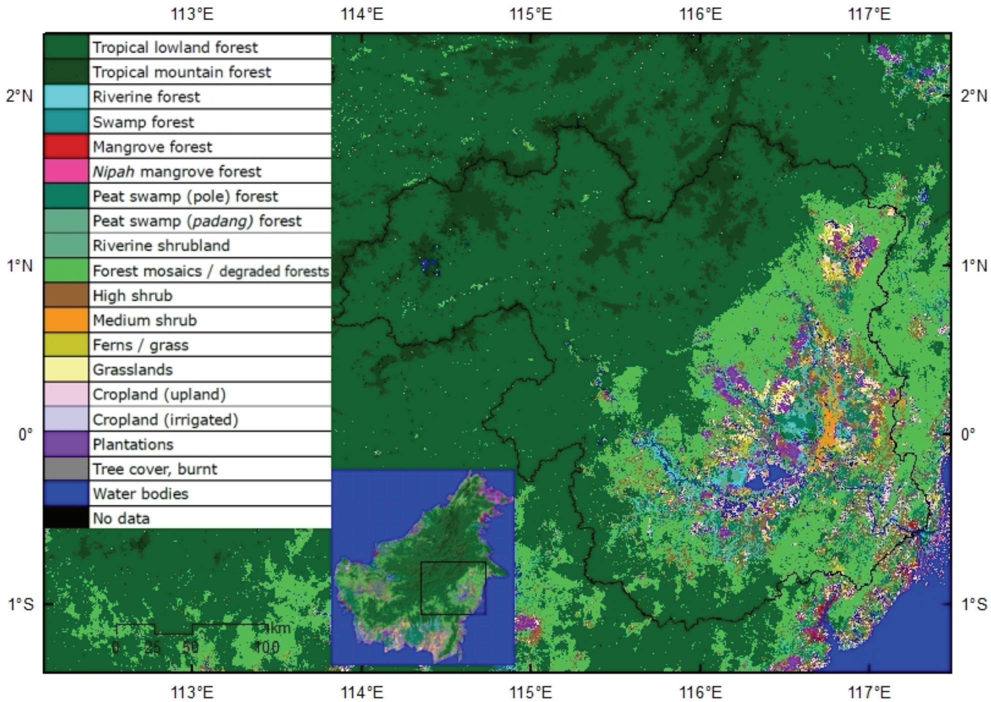

Fig. 1. Land use – land cover map of the Mahakam river basin based on PALSAR images of 2007 (Hoekman et al., 2010). The black line indicates catchment boundary.

HESSD
8, 11519–11552, 2011

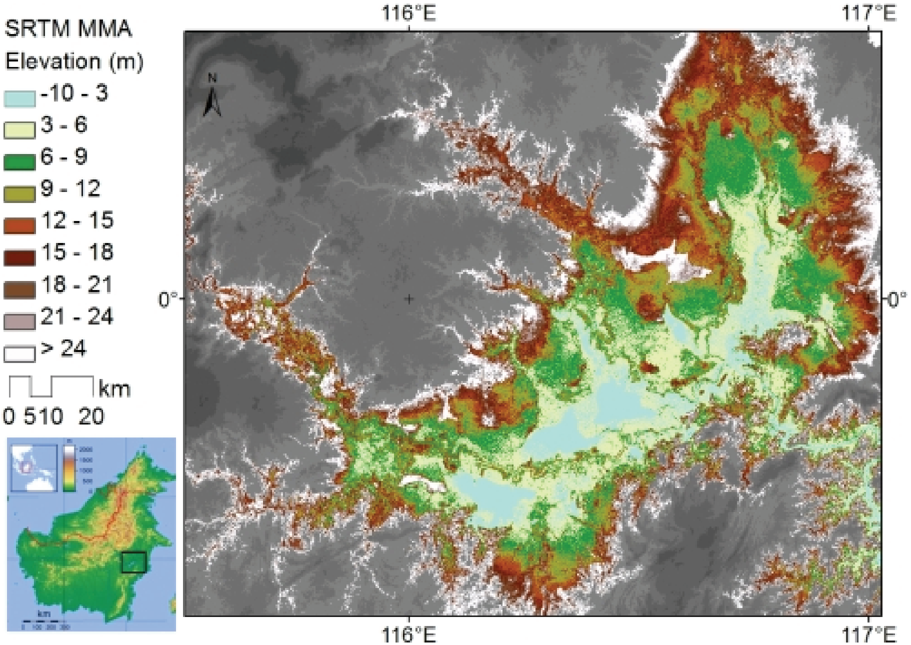

Fig. 2. Study area in East Kalimantan with colour coded SRTM digital elevation model for the middle Mahakam lowland area.

HESSD
8, 11519–11552, 2011

Flood frequency mapping of a tropical lowland

H. Hidayat et al.

Fig. 3. River bank overtopping in Penyinggahan during the high water event in March 2009. The red line indicates water level mark on trees from previous flood event.

HESSD
8, 11519–11552, 2011

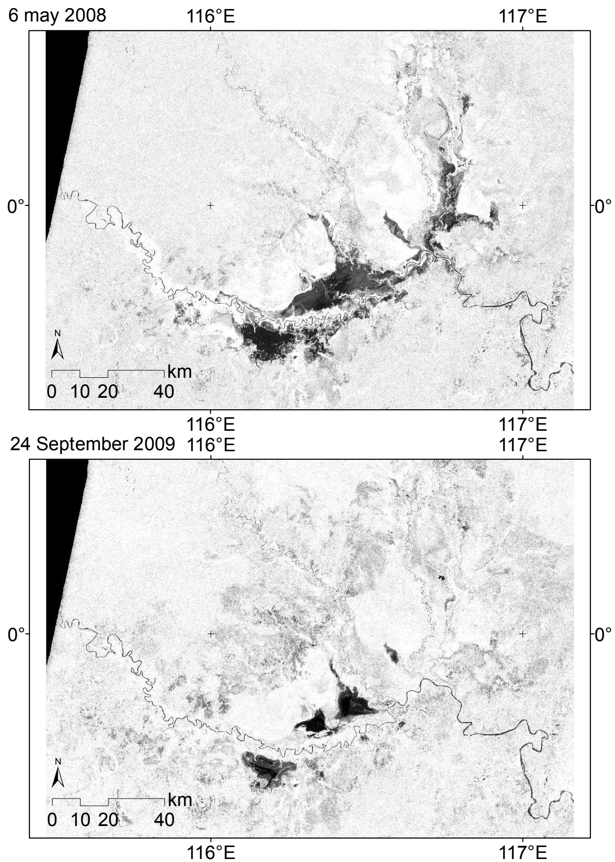

Fig. 4. PALSAR images of the middle Mahakam area during wet season (top) and dry season (bottom). Dark areas are open water extent, bright area indicates inundation under vegetation cover.

HESSD
8, 11519–11552, 2011

Title Page
Abstract | Introduction
Conclusions | References
Tables | Figures
◀I | ▶I
◀ | ▶
Back | Close
Full Screen / Esc
Printer-friendly Version
Interactive Discussion

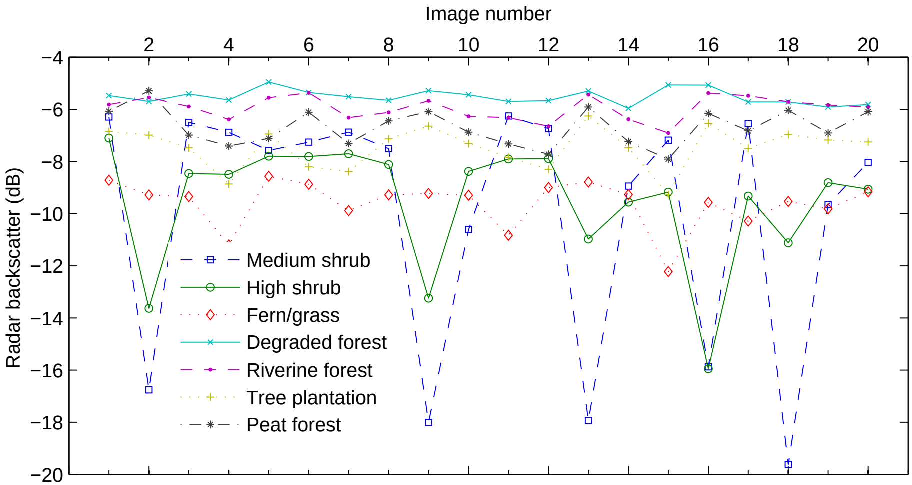

Fig. 5. Radar backscatter of land cover classes in the Mahakam lake area. Image numbers correspond with image acquisition date in Table 1.

HESSD
8, 11519–11552, 2011

Flood frequency mapping of a tropical lowland

H. Hidayat et al.

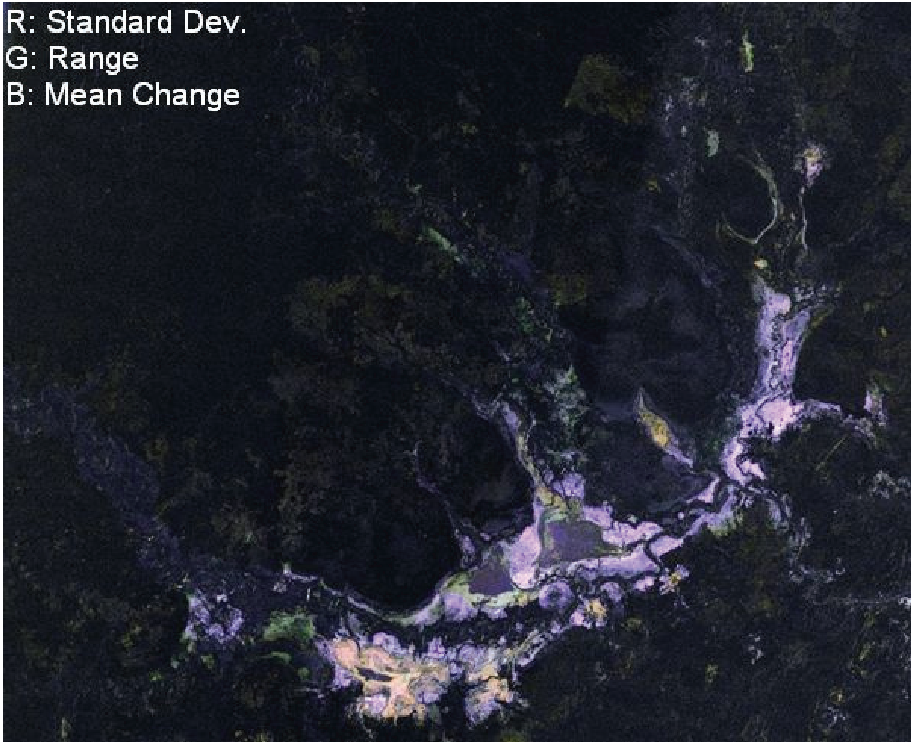

Fig. 6. Result of temporal analysis of 20 PALSAR images of period 19 March 2007 until 27 September 2010. Light purple indicates the regularly inundated shrubland, green indicates reeds/sedges, yellow at the southern lake indicates rice growing areas in years when flooding is not too high.

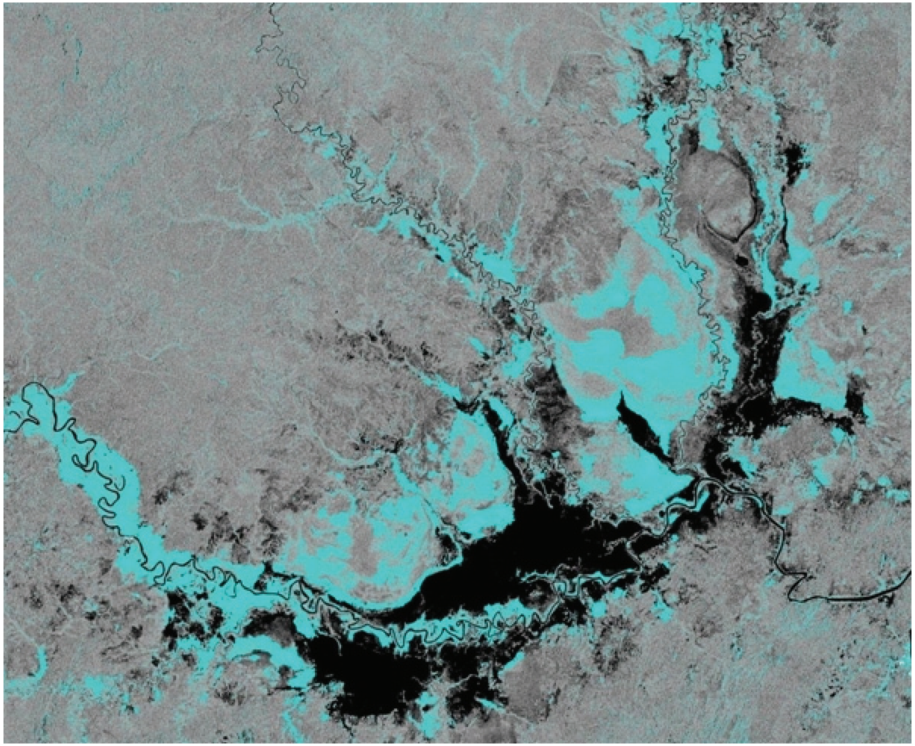

Fig. 7. Inundation extent obtained by averaging three images in wet period (4 May 2007, 22 December 2008, and 9 February 2010). Dark area indicates open water inundation extent, cyan indicates flooding under vegetation.

HESSD

8, 11519–11552, 2011

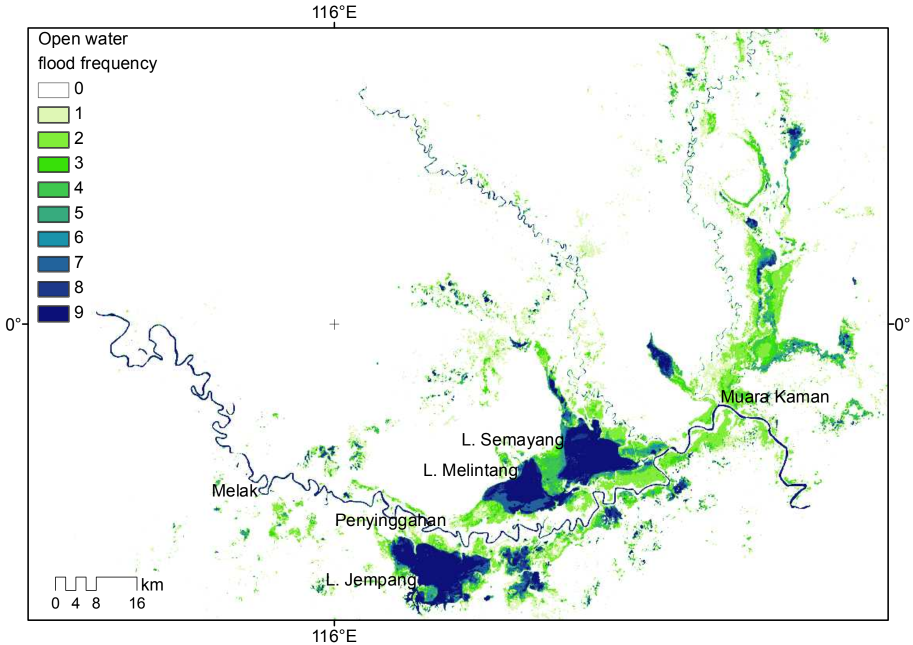

Fig. 8. Flood frequency map of middle Mahakam area obtained from the filtered (enhanced Lee) PALSAR images of 2008–2009.

HESSD
8, 11519–11552, 2011

Flood frequency mapping of a tropical lowland

H. Hidayat et al.

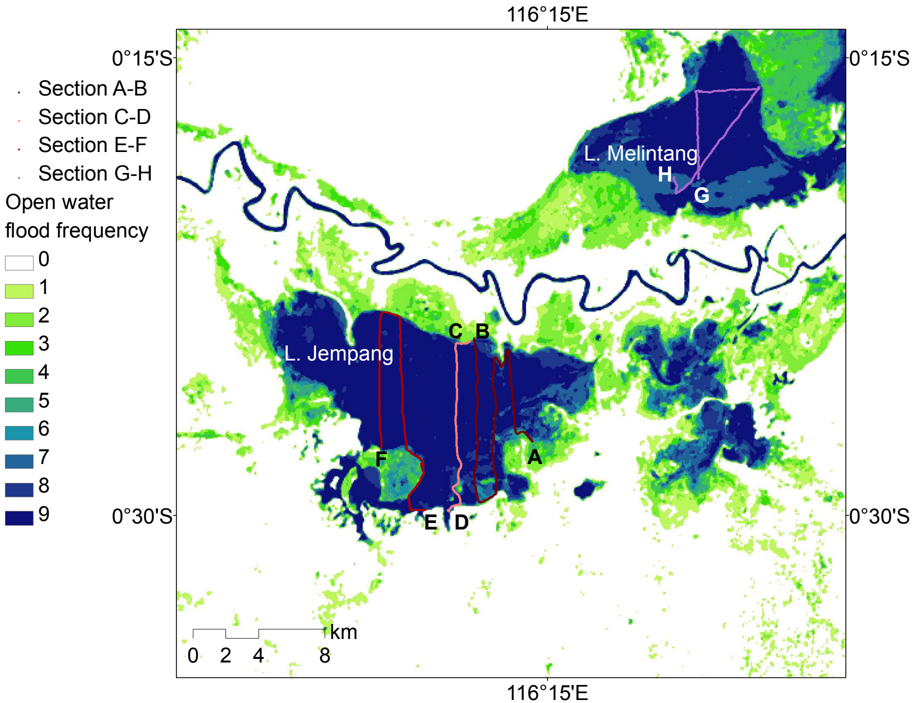

Fig. 9. Bathymetry measurements in Lake Jempang and Lake Melintang plotted on the flood frequency map from nine PALSAR images of 2008–2009.

HESSD
8, 11519–11552, 2011

Flood frequency mapping of a tropical lowland

H. Hidayat et al.

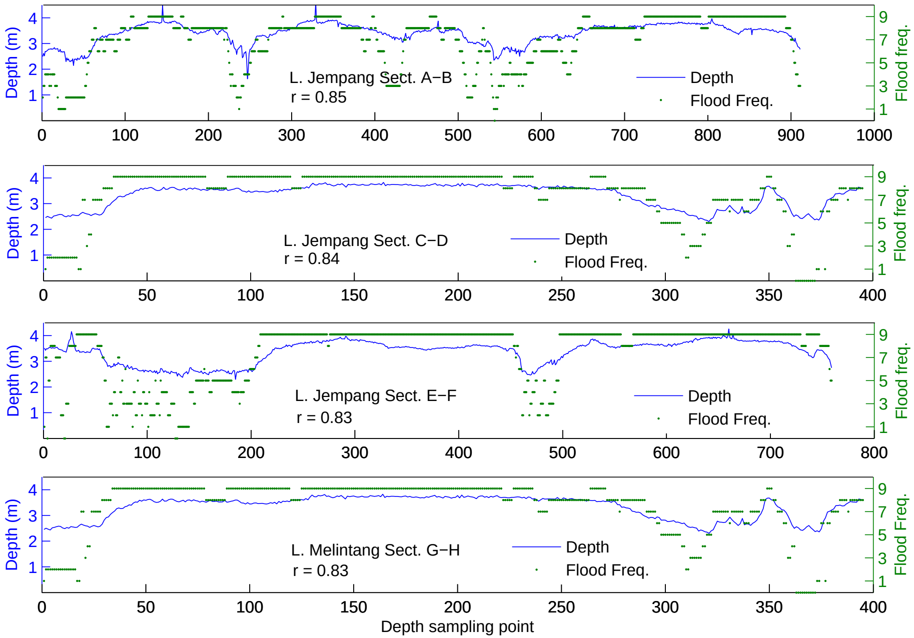

Fig. 10. Lake depth vs. flood frequency from nine PALSAR images of 2008–2009, r values indicate correlation coefficient.

HESSD
8, 11519–11552, 2011

Flood frequency mapping of a tropical lowland

H. Hidayat et al.

Title Page
Abstract
Introduction
Conclusions
References
Tables
Figures
◀
▶
Back
Close
Full Screen / Esc
Printer-friendly Version
Interactive Discussion

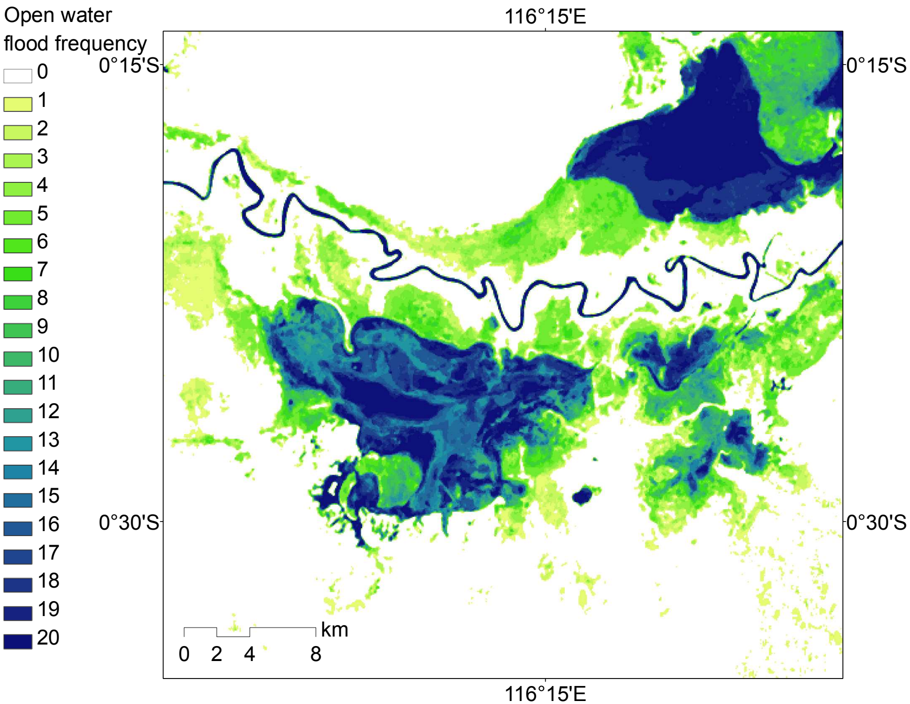

Fig. 11. Flood frequency map from 20 PALSAR images of 2007–2010 zoomed in lakes area.

HESSD
8, 11519–11552, 2011

Flood frequency mapping of a tropical lowland

H. Hidayat et al.

Fig. 12. Bulks of floating vegetation flushed off Lake Jempang drifting downstream during lake emptying period.

HESSD
8, 11519–11552, 2011

HESSD

8, 11519–11552, 2011

Flood frequency mapping of a tropical lowland

H. Hidayat et al.

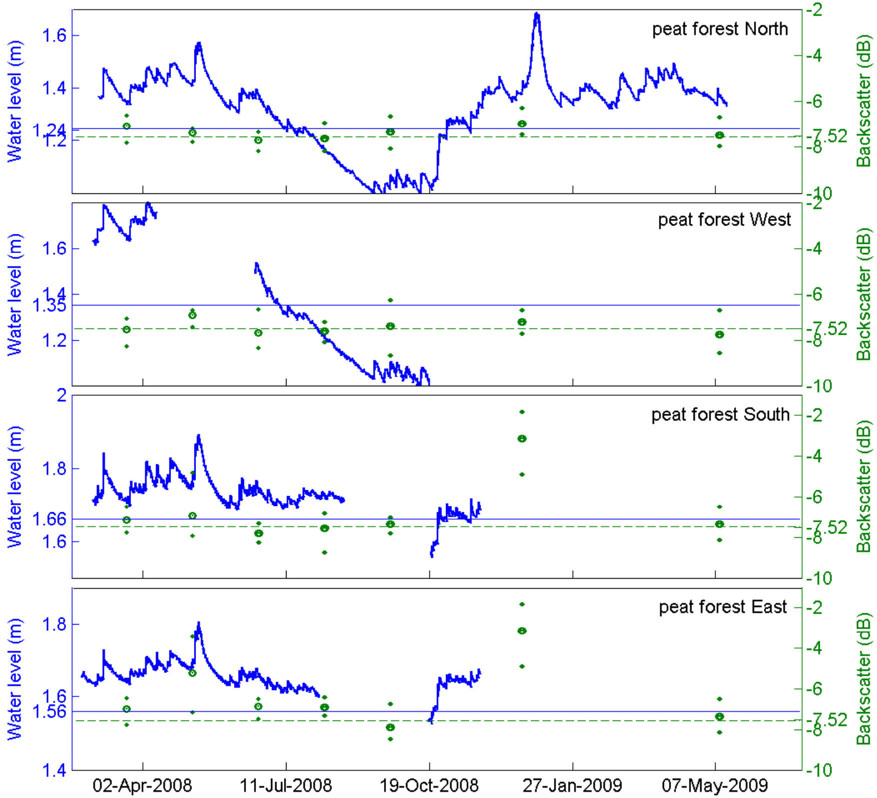

Fig. 13. Water level and radar backscatter return values obtained from a block of nine pixels at the water level gauge locations in the peat forest near Lake Melintang. Blue lines indicate ground levels at the gauge locations. Water levels are with respect to the subterrain position of each pressure sensors. Green circles, upper and lower dots indicate mean, maximum and minimum backscatter values, respectively. The dashed green line indicates the ground level for the radar backscatter return.

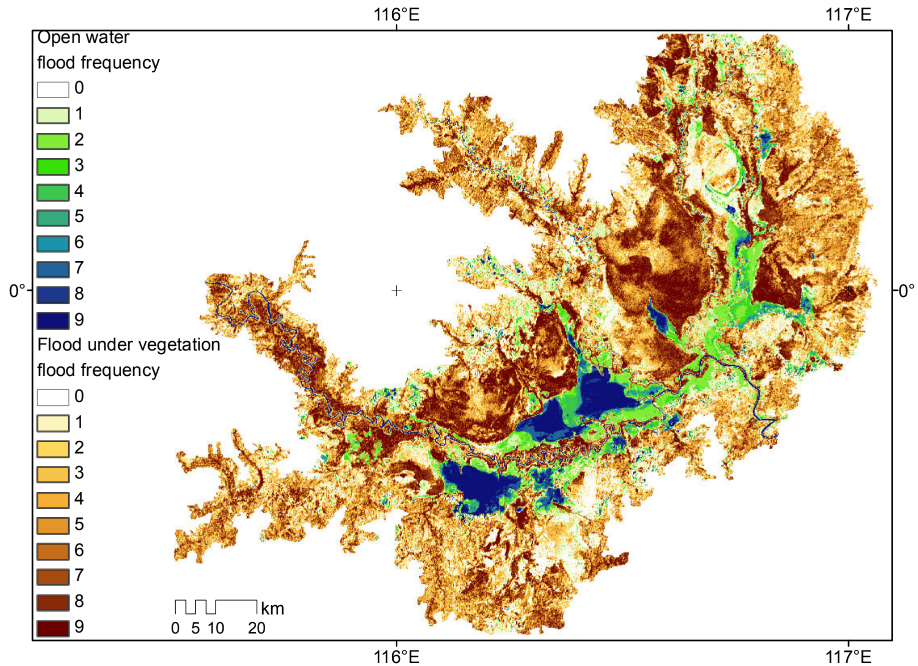

Fig. 14. Composite flood frequecy map of the Kutai wetlands from nine PALSAR images for 2008/2009 as an overlay of results for open water and for inundation under vegetation cover.

HESSD
8, 11519–11552, 2011

Flood frequency mapping of a tropical lowland

H. Hidayat et al.

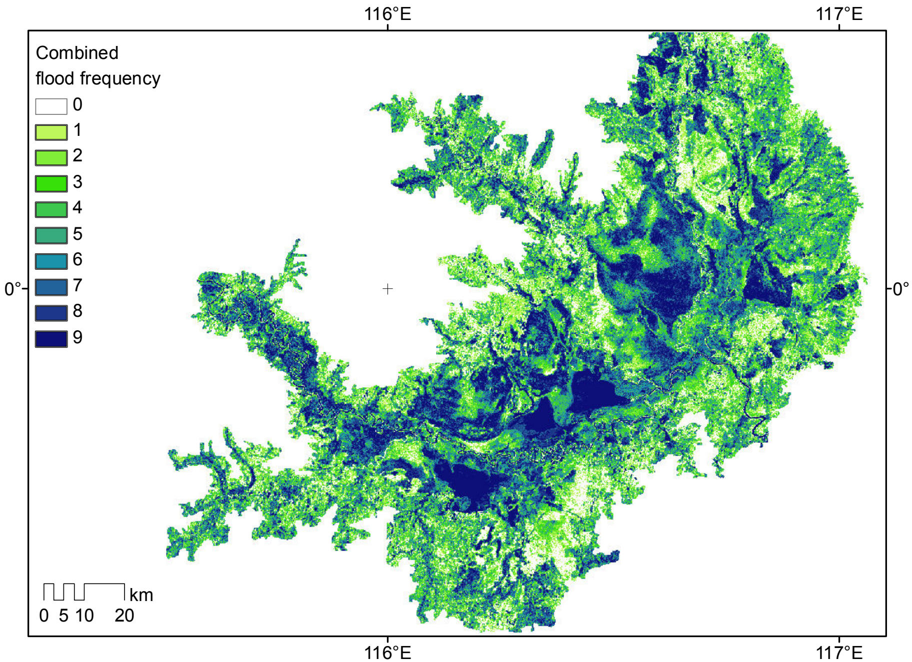

Fig. 15. Combined flood frequency map of the Kutai wetlands from nine PALSAR images for 2008/2009, counting the total number of flood cases per pixel, which represents open water and flooding under vegetation.

HESSD
8, 11519–11552, 2011